ISSN 1063-7834, Physics of the Solid State, 2013, Vol. 55, No. 4, pp. 829–836. © Pleiades Publishing, Ltd., 2013.
Original Russian Text © A.A. Titov, V.F. Balakirev, A.S. Volegov, A.E. Kar'kin, A.N. Titov, S.G. Titova, 2013, published in Fizika Tverdogo Tela, 2013, Vol. 55, No. 4, pp. 759–765.

PHASE TRANSITIONS

Structure and Properties of the Intercalation Compound Fe_xTiTe_2

A. A. Titov[a], V. F. Balakirev[b], A. S. Volegov[c], A. E. Kar'kin[a], A. N. Titov[a, c, *], and S. G. Titova[b, **]

[a] *Institute of Metal Physics, Ural Branch of the Russian Academy of Sciences, ul. Sofii Kovalevskoi 18, Yekaterinburg, 620990 Russia*

* *e-mail: antitov@mail.ru*

[b] *Institute of Metallurgy, Ural Branch of the Russian Academy of Sciences, ul. Amundsena 101, Yekaterinburg, 620016 Russia*

** *e-mail: sgtitova@mail.ru*

[c] *Ural Federal University named after the First President of Russia B.N. Yeltsin (Ural State Technical University–UPI), ul. Mira 19, Yekaterinburg, 620002 Russia*

Received July 4, 2012

Abstract—The Fe_xTiTe_2 system, which belongs to the class of materials with the electronic spectrum containing below the Fermi level the band of localized states with a strong temperature dependence of the band width, has been investigated experimentally. Heating of the material leads to a broadening of the band of localized states. When the top of this band crosses with the Fermi level, the effect of retrograde solubility is observed in the system; i.e., the metal precipitates to the composition ensuring the absence of increase in the Fermi energy during heating. The influence of the band of localized states on the structure of the material and its magnetic and electrical properties has been analyzed.

DOI: 10.1134/S106378341304032X

1. INTRODUCTION

In intercalation materials with transition metals, which form multiply charged ions, the intercalation leads to the formation of a covalent complex consisting of the inserted metal and the nearest environment of the host lattice with the electronic spectrum containing dispersionless bands below the Fermi level [1, 2]. The energy in these bands is related to the size of the covalent complex [3]. The heating of the material, which leads to a thermal smearing of the atomic configuration of the covalent complex, provides a strong temperature dependence of the width of the dispersionless bands. It was experimentally established that, in the Fe_xTiSe_2 system, there is a correlation between the specific features of the electronic structure of the material (the presence of the band of localized states with a strong temperature dependence of the band width in the electronic spectrum) and the phase diagram [4, 5]; i.e., there is the observed effect of retrograde solubility. The heating of the material results in a broadening of the band of localized states, and when the top of this band crosses with the Fermi level, metallic iron precipitates to the composition ensuring the absence of increase in the Fermi energy as a function of the temperature. Since this mechanism, which was confirmed experimentally in [4, 5], is not related to the chemical nature of the object, it is obvious that such effects should be observed whenever the material exhibits similar features of the electronic structure. An important feature of the material, which makes it possible to observe the retrograde solubility, lies in the fact that the band of localized states is close to the Fermi level so that the top of the band can reach the Fermi level in a reasonable range of temperatures no higher than the temperature of thermal dissociation of localized states. The analysis of the available data on angle-resolved photoemission spectroscopy of intercalation compounds of titanium dichalcogenides has demonstrated that this condition is satisfied by the Fe_xTiTe_2 system [1]. For the Fe_xTiTe_2 system, on the projection of the Brillouin zone in the direction $M'-\Gamma-M$, there are two dispersionless bands with low binding energies of -0.03 and -0.30 eV. At the same time, for the Fe_xTiSe_2 system in the same section of the Brillouin zone, there is only one band with a binding energy of -0.3 eV [2]. This suggests the existence of the effect of retrograde solubility for the Fe_xTiTe_2 system and gives an opportunity to investigate the influence of the contribution from more than one band on the phase diagram.

The Fe_xTiTe_2 system was previously studied using the isothermal section method at a temperature of 900°C and demonstrated an unusually low iron solubility of no more than 25 mol % [5]. This indirectly indicates the possible existence of the retrograde solubility of iron in $TiTe_2$. In the present work, we con-

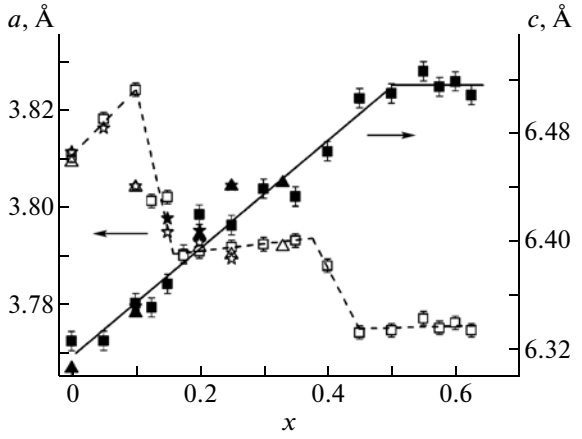

Fig. 1. Dependences of the unit cell parameters a and c for the Fe_xTiTe_2 compound on the iron content according to the results obtained for two independent series of samples. Squares are our data; triangles and asterisks are the data taken from [6] and [10], respectively.

structed several isothermal sections, which made it possible to determine the boundary of solubility of iron in $TiTe_2$.

2. SAMPLE PREPARATION AND EXPERIMENTAL TECHNIQUE

The crystals were grown using the standard technique of ampoule synthesis from preliminarily prepared powdered titanium telluride $TiTe_2$ and granulated carbonyl iron reduced in a hydrogen flow at a temperature of 750°C. It should be noted that, in the case of materials with a retrograde solubility, their synthesis has ceased to be a trivial task. The point is that, by choosing a high temperature, we can encounter the thermodynamic limitations of the solubility, whereas the solubility at low temperatures is limited by kinetic difficulties. Therefore, at the first stage, we carried out the initial synthesis at the highest temperature that could be withstood by quartz ampoules, i.e., at 1100°C. The idea consisted in using a non-quasibinarity of intercalation systems, which manifested itself in the influence of the concentration of the precipitated intercalant on the position of the equilibrium boundary [6]. In other words, at such a high temperature, iron must necessarily react if not with $TiTe_2$ then with the vapor of dissociated tellurium over the surface. Indeed, this annealing for a week ensured the absence of large granules of the initial iron, even though, in many cases, the samples were contaminated with dispersed particles of metallic iron and iron tellurides. The samples thus obtained, after careful grinding and subsequent pressing, were subjected to homogenizing annealings at specified temperatures with the aim of constructing isothermal sections of the region of iron solubility in $TiTe_2$. A total of five isothermal sections were constructed at temperatures of 1100, 900, 800, 776, and 550°C. The duration of homogenizing annealing was varied from one week at high temperatures (1100–800°C) to two weeks at low temperatures (776–550°C). The homogeneity of the samples was controlled using the X-ray powder diffraction analysis (Shimadzu XRD 7000 Maxima diffractometer, CuK_α radiation, graphite monochromator). The temperature dependences of the magnetic properties were measured on a Quantum Design MPMS-XL-7 EC magnetometer in a constant magnetic field $H = 10$ kOe. The measurement error did not exceed 1%. The rate of change in temperature was 2 K/min. The error in the determination of the temperature was less than ±1 K. The electrical conductivity was measured on single-crystal samples in the Montgomery geometry [7].

The single crystals were grown by the gas-transport reaction method with iodine used as a carrier gas. Details of this method were described in [8].

3. RESULTS AND DISCUSSION

3.1. Crystal Structure

The performed investigation has revealed that neither the iron ordering nor the associated lowering of the symmetry are observed over the entire homogeneity region of the Fe_xTiTe_2 compositions prepared at all temperatures of annealings. The crystal structure of all the homogeneous samples, as well as the parent compound $TiTe_2$, can be described by the space group $P\bar{3}m1$. When the iron concentration exceeds the solubility limit, the X-ray diffraction patterns contain lines of metallic iron. The full-profile analysis of the X-ray diffraction patterns with the GSAS software package [9] for homogeneous compositions has demonstrated that iron atoms are located in the so-called van der Waals gap and octahedrally coordinated by tellurium.

The concentration dependences of the unit cell parameters a and c are shown in Fig. 1. It is easy to see that the dependence can be divided into several parts with a fundamentally different behavior: an increase in the unit cell parameter c with increasing concentration of iron is observed in the iron concentration ranges $0 < x < 0.1$, $0.175 < x < 0.350$, and $0.45 < x < 0.65$, whereas in the iron concentration ranges $0.100 < x < 0.175$ and $0.35 < x < 0.45$, the unit cell parameter c decreases with an increase in the iron concentration. It should be noted that, in general, the unit cell parameters obtained in the present study coincide with the data reported in earlier papers [6, 10], with the only difference that, in those works, the complex dependence $c(x)$ was not revealed because of the very large step in the concentration.

The cause for the observed decrease in the unit cell parameter $c(x)$ in the direction perpendicular to the titanium dichalcogenide layers in intercalation mate-

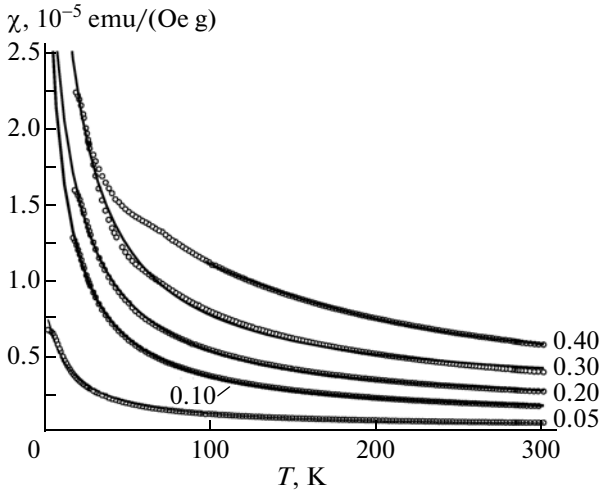

Fig. 2. Temperature dependences of the magnetic susceptibility of the Fe_xTiTe_2 samples (the iron content x is indicated near the curves). Solid lines show the approximation by the Curie–Weiss law.

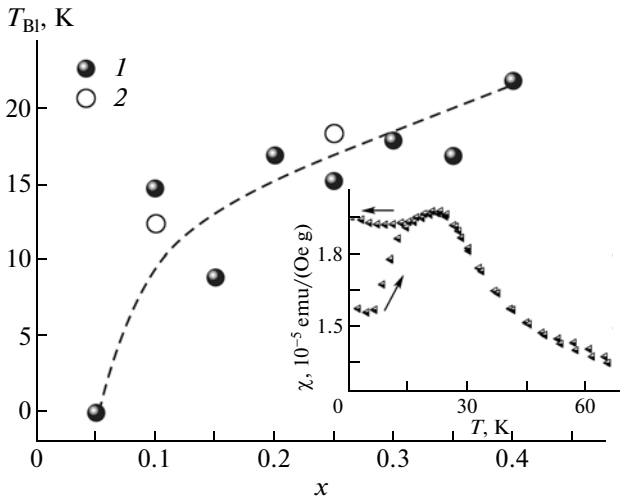

Fig. 3. Concentration dependence of the blocking temperature of the magnetic moments for the Fe_xTiTe_2 system according to (*1*) data of this work and (*2*) data taken from [12]. The inset shows the temperature dependence of the magnetic susceptibility in the magnetic field $H = 10$ kOe for the $Fe_{0.4}TiTe_2$ sample during heating (cooling without field, ZFC) and the subsequent cooling in the magnetic field (FC). The direction of the process is shown by arrows.

rials is well known: it is the formation of covalent centers due to the hybridization of the $M3d$/Ti$3d$ states (where M is the intercalant) [11]. The cause for the observed increase in the unit cell parameter $c(x)$ can be either the ionic nature of the intercalant–lattice chemical bond, as is observed in materials intercalated with alkali metals [12, 13], or the formation of hybrid states between the $3d$ states of the intercalant and the chalcogen, which is observed in the Mn_xTiSe_2 system [14]. However, for the Fe_xTiTe_2 system, the experimental data on resonance photoemission spectroscopy [1] clearly indicate a hybrid nature of the Fe$3d$/Ti$3d$ states of the dispersionless bands. This suggests that there is a correlation between the concentration dependences of the unit cell parameters and the specific features of the charge transfer between iron and the $TiTe_2$ lattice.

3.2. Magnetic Measurements

As was noted above, the observed increase in the unit cell parameter $c(x)$ can be associated only with the filling of the dispersionless bands of the hybrid Fe$3d$/Ti$3d$ states and the dependence of the concentration of iron–lattice covalent centers on the iron content. It is obvious that, in this case, the density of states at the Fermi level should correlate with the concentration dependences of the lattice parameters. The density of states at the Fermi level can be obtained from the temperature-independent contribution to the magnetic susceptibility. However, this density of states cannot be directly obtained because of the presence of magnetic iron atoms: it is determined as one of the parameters used for the optimization of the temperature dependence of the magnetic susceptibility by varying the concentrations of the intercalated iron.

The experimental temperature dependences of the magnetic susceptibility of the Fe_xTiTe_2 samples are shown in Fig. 2. At low temperatures ($T < 50$ K), these dependences exhibit a characteristic behavior of the spin-glass or cluster-glass state, which was observed previously in [15] (see inset in Fig. 3). The temperature of bifurcation (divergence) of the ZFC- and FC-curves in the temperature dependence of the magnetic susceptibility in the case of the spin-glass state corresponds to the blocking temperature of the magnetic moments T_{Bl}. The concentration dependence of the blocking temperature of the magnetic moments T_{Bl} of the Fe_xTiTe_2 system is shown in Fig. 3. As can be seen, this temperature increases with an increase in the iron concentration and reaches 20 K. At temperatures above $T \sim 50$ K, the magnetic susceptibility χ is approximated by the Curie–Weiss law $\chi = \chi_0 + \dfrac{C}{T - \Theta}$, where C is the Curie constant, from which the effective magnetic moment μ_{eff} can be calculated; T is the temperature; Θ is the paramagnetic Curie temperature; and χ_0 is the temperature-independent contribution, which combines the Pauli paramagnetic contribution of free electrons and the diamagnetic contribution of the filled shells. Since the diamagnetic contribution is significantly less than the Pauli paramagnetic contribution and, moreover, is ensured predominantly by the filled shells of the lattice atoms (the fraction of the iron atoms does not exceed 15% of the total number of atoms), this contribution can be disregarded.

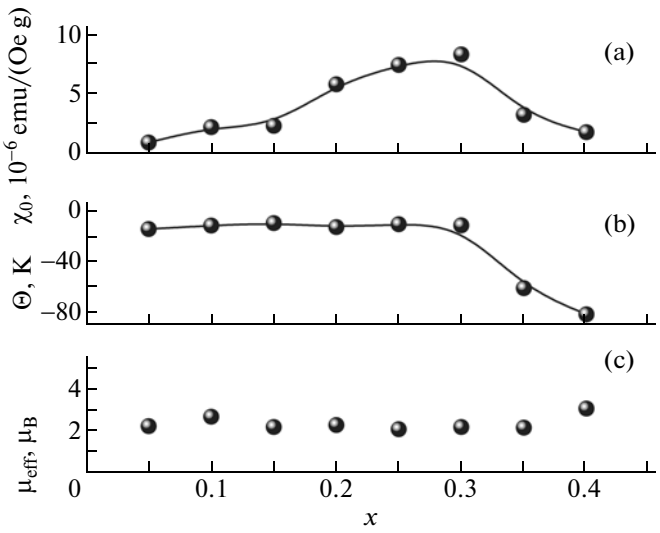

Fig. 4. Results of the approximation of the temperature dependence of the magnetic susceptibility for the Fe_xTiTe_2 system (Fig. 2) according to the Curie–Weiss law: (a) the temperature-independent contribution to the magnetic susceptibility χ_0, (b) the paramagnetic Curie temperature Θ, and (c) the effective magnetic moment μ_{eff} of the Fe^{2+} ions.

The concentration dependences of the parameters of the approximation of the experimental dependences $\chi(T)$ for different iron concentrations are shown in Fig. 4. The effective magnetic moment μ_{eff} is almost independent of the iron concentration. This is rather strange if we consider the correlation observed for all the intercalation compounds of titanium dichalcogenides between the behavior of the lattice parameter $c(x)$, which reflects the degree of hybridization of the Ti3*d* states with the 3*d* states of the intercalated metal, and the effective magnetic moment μ_{eff} [16]. The barely noticeable maximum of the effective magnetic moment μ_{eff} near the iron concentration $x \sim 0.1$ coincides, however, with the maximum in the curve of the concentration dependence of the lattice parameter $c(x)$, but this is the only coincidence. It seems likely that, over the entire iron solubility region, the material is on the verge of stability of covalent complexes, which ensures minor changes in the effective magnetic moment μ_{eff}. The paramagnetic Curie temperature Θ is almost independent of the iron concentration in the temperature range significantly above the temperature of transition to the spin-glass or cluster-glass state in the region $x < 0.3$. Most likely, this indicates a weakness of the magnetic interaction in the subsystem of the intercalant. At a higher iron concentration, the paramagnetic Curie temperature is observed to increase, which suggests an enhancement of the interaction in the iron sublattice. The negative sign indicates that the antiferromagnetic interactions dominate in the iron sublattice, which is well consistent with the behavior of the magnetic susceptibility near the blocking temperature of the magnetic moments (Fig. 4).

The concentration dependence of the temperature-independent contribution χ_0 demonstrates a correlation with the behavior of the concentration dependence of the lattice parameter $c(x)$: the value of χ_0 increases in the range of the increasing dependence $c(x)$, and it either does not increase (for $x = 0.10$–0.25) or decreases in the range of the decreasing dependence $c(x)$. This behavior seems to be natural if the temperature-independent contribution χ_0 is related to the contribution of free electrons. Actually, as was shown in [17], the hybridization of the Ti3*d* states with the states of the intercalated metal leads to a "switching" of titanium states from the conduction band into the band (or bands) of hybrid states lying below the Fermi level. Therefore, the formation of covalent complexes should decrease the density of states of the conduction band. The increase in the temperature-independent contribution χ_0 can also be associated with the fact that the iron states or hybrid Fe3*d*/Ti3*d* states appear to be directly at the Fermi level, which can be caused by the dependence of the width of the bands of hybrid states on the iron concentration. This dependence was discussed in [16], where it was shown that the attainment of percolation thresholds in the sublattice of covalent complexes and in the sublattice of the intercalant affects the width of the bands of the corresponding states. Moreover, it was assumed that each sublattice generates only one band. The presence of two bands of localized states in the Fe_xTiTe_2 system can induce a similar effect with the participation of each of the bands. Therefore, we can expect the presence of two minima in the dependence $c(x)$, which is actually observed in the experiment.

3.3. Electronic Properties

The results of measurements of the electrical resistivity and Hall coefficient are presented in Figs. 5–7. It is worth noting that the Hall coefficient has a positive sign over the entire concentration and temperature ranges, as in the case of the parent compound $TiTe_2$ [18]. This indicates that the dominant hole carriers retain their position despite the intercalation of the metal and the formally donor doping. This situation becomes possible in the case where the transfer of intercalant electrons occurs not into the conduction band of the host lattice, but into the band of hybrid states, which is observed in angle-resolved photoemission spectroscopy. At the same time, the temperature dependence of the Hall coefficient R_H of the Fe_xTiTe_2 single crystals radically changes as compared to $TiTe_2$. The inflection attributed to the competition of the contributions from different parts of the Fermi surface disappears in this dependence, and it acquires a monotonic behavior. Such a transformation becomes possible if there appears a dominant type of charge

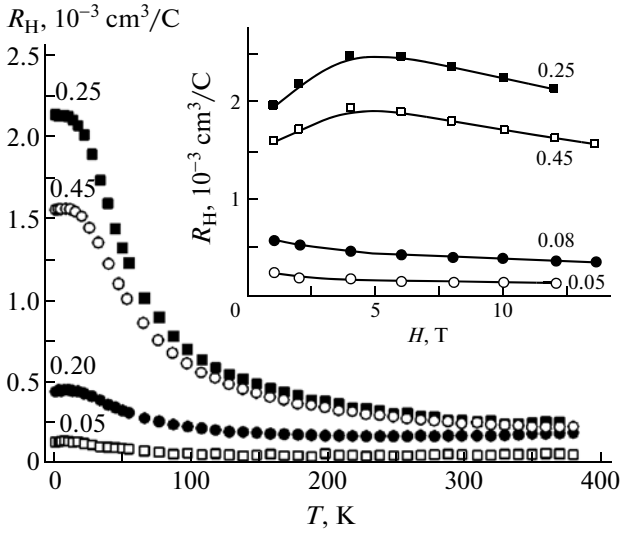

Fig. 5. Temperature dependences of the Hall coefficient of the Fe_xTiTe_2 single crystals. The inset shows the field dependences of the Hall coefficient. The iron content is indicated near the curves.

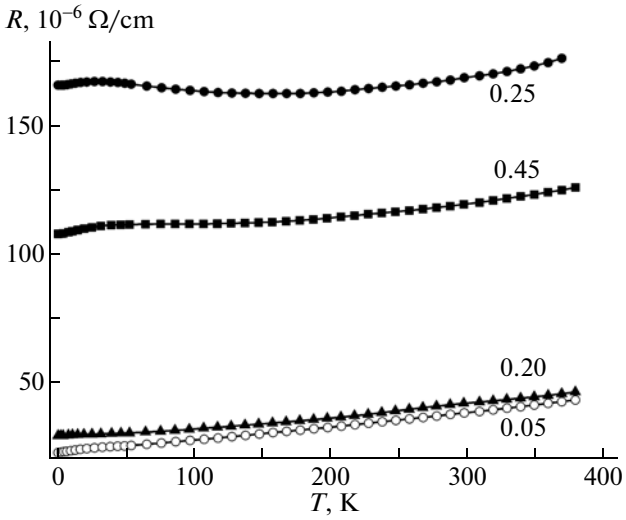

Fig. 6. Temperature dependences of the electrical resistivity of the Fe_xTiTe_2 single crystals along the basal plane. The iron content is indicated near the curves.

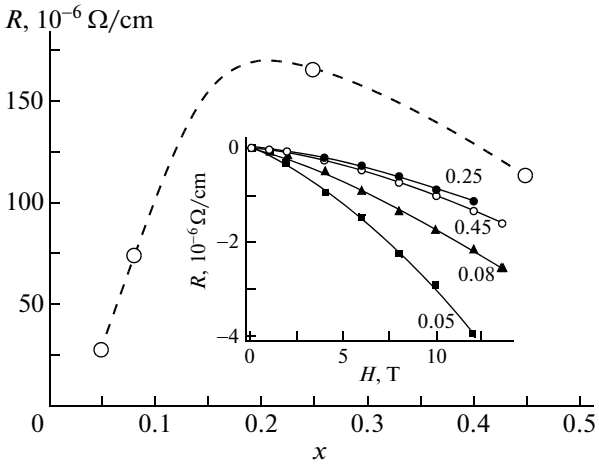

Fig. 7. Concentration dependences of the electrical resistivity of the Fe_xTiTe_2 single crystals measured at 100 K. The inset shows the field dependences of the electrical resistivity. The iron content is indicated near the curves.

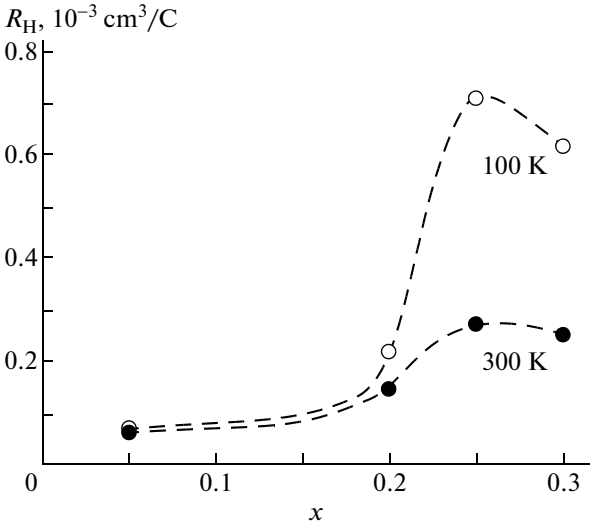

Fig. 8. Concentration dependences of the Hall coefficient measured at temperatures of 100 and 300 K.

carriers. Obviously, this situation can arise as a result of the depletion of the conduction band due to the capture of electrons into the band of hybrid states, so that holes in the valence band are in the dominant position.

At low temperatures, which correspond to the state of magnetic ordering, the Hall constant demonstrates the field and temperature dependences that are characteristic of the anomalous Hall effect (see Fig. 5 and inset to it). In the temperature range $T > T_{Bl}$, the behavior of the Hall constant is characteristic of conventional metals. This is consistent with the assumption that the charge carriers have an itinerant nature.

The temperature dependences of the electrical resistivity (Fig. 6) have a characteristic shape for metals over the entire concentration range; however, the slope of these dependences is relatively small. This can be associated with the presence of several types of charge carriers with different mobilities in the single crystal. The concentration dependence of the electrical resistivity (Fig. 7) exhibits a maximum for the same

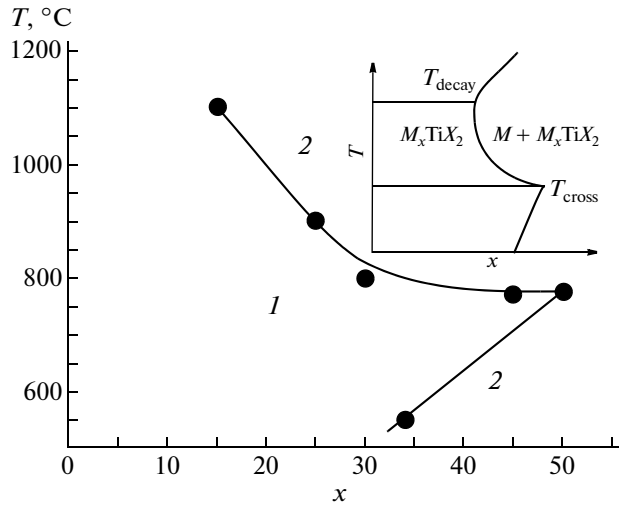

Fig. 9. Temperature dependence of the limiting solubility of iron in $TiTe_2$: (*1*) single-phase state of Fe_xTiTe_2 and (*2*) mixture of the phases Fe + Fe_xTiTe_2. The inset shows the schematic phase diagram of materials with the more than half-filled impurity band of localized states below the Fermi level, which was proposed in [4].

composition as for the Hall constant (Fig. 8). It seems likely that this region of concentrations is characterized by a decrease in the concentration of dominant carriers. The strong temperature dependence of the Hall coefficient near the composition with $x = 0.25$ indicates the electron exchange between the localized electrons of the band of hybrid states and the extended states at the Fermi level. It should be noted that, at the same composition, the lattice parameter c has a minimum, which corresponds to the maximum concentration of covalent complexes responsible for the formation of the band of hybrid states. It is evident that the concentration of conduction electrons at this composition should also have a minimum value. This explanation is confirmed by the fact that the Pauli contribution to the magnetic susceptibility also passes through a maximum in the vicinity of this composition (Fig. 4). Since the highest density of states is associated with the band of hybrid states, the aforementioned fact suggests that, at this composition, the concentration of localization centers has a maximum value.

The magnetoresistance (see inset in Fig. 7) has a negative sign, as has been observed in many materials intercalated with transition metals that provide spin polarization of the hybrid *M*3*d*/Ti3*d* states [15, 19]. Since the temperature dependences of the magnetoresistance do not respond to magnetic phase transitions, it seems logical to relate this quantity to the influence of the spin polarization of hybrid states. This suggests that the two observed dispersionless bands can be formed as a result of the spin polarization of the Fe3*d*/Ti3*d* states.

Thus, the kinetic data have demonstrated that the most probable mechanism of influence of the hybridization of the Fe3*d*/Ti3*d* states on the electrical properties of the system is the electron exchange between the band of these states and the bands containing free charge carriers.

3.4. Phase Diagram

The Fe/Fe_xTiTe_2 equilibrium boundary is shown in Fig. 9. It is clearly seen that this boundary can be divided into two sections corresponding to temperatures below and above 770°C. In the low-temperature region, the solubility of iron, as usual, increases with an increase in the temperature, whereas in the high-temperature region, the effect of retrograde solubility takes place. This type of phase diagram exactly corresponds to the scheme of phase diagrams of the materials with localized states below the Fermi level [4] (see inset in Fig. 9). According to the scheme proposed in [4], the low-temperature part corresponds to the presence of a gap between the top of the band (or bands) of localized states and the Fermi level. The point of intersection of the parts corresponds to the crossing of the top of these bands with the Fermi level. The concave shape of the solubility boundary reflects a decreasing contribution of the localized states with a decrease in the concentration of the dissolved iron.

A similar phase diagram was obtained for the Fe–Fe_xTiSe_2 system [5]. However, this diagram contained the high-temperature boundary of the stability region of the (Fe + Fe_xTiSe_2) phase mixture but had no region of normal solubility. Apparently, this corresponds to the high-temperature part of the schematic phase diagram, whereas the phase diagram of the Fe–Fe_xTiTe_2 system corresponds to the low-temperature part of the schematic diagram. This can be explained by the stronger interaction between the $TiTe_2$ layers as compared to $TiSe_2$, which leads to a higher stability of covalent complexes in the Fe_xTiTe_2 system as compared to the Fe_xTiSe_2 system. In actual fact, if the position of the solubility boundary is determined by the thermal broadening of the band of localized states, the increase in the elasticity of the lattice should slow down this process and thereby stabilize the covalent complexes. A higher elasticity of $TiTe_2$ as compared to $TiSe_2$ is indicated by a lower compressibility of $TiTe_2$ [20]. Experimentally, this is manifested in the observed difference between the dislocation structures [21]: the concentration of dislocations in $TiTe_2$ is significantly lower than that in $TiSe_2$.

It seems likely that the role of elasticity of the lattice can also manifest itself in the shape of the solubility boundary. Indeed, as was shown in [22], the intercalation, which leads to a compression of the lattice in the direction along the normal to the basal plane, causes an increase of the Debye temperature and, hence, an increase in the elasticity of the lattice.

Therefore, the extraction of iron, which in general ensures an increase in the lattice parameter c, should decrease the elasticity of the lattice. However, on the other hand, as was noted above, this should lead to a decrease in the thermal stability of covalent centers and, consequently, should accelerate their degradation during heating. These factors will provide a concave shape of the solubility boundary, which is actually observed in the experiment. Probably, the effect manifests itself in the case where the change in the elasticity is large enough. When this is not the case, the solubility boundary can also have a convex shape, as was observed in the $Fe-Fe_xTiSe_2$ system.

Thus, we can conclude that the form of the phase diagram of an intercalation material that has localized states at the Fermi level depends both on the binding energy of the bands of localized states and on the elasticity of the host lattice, which determines the dynamics of thermal expansion. When the temperature range is chosen above the stability boundary of the retrograde solubility region or below the temperature of retrograde solubility, the phase diagram has the same form as in the case of classical diagrams of solid solutions. Apparently, this is also true for the $Fe-Fe_xTiS_2$ system: the TiS_2 lattice has even a lower elasticity than the $TiSe_2$ lattice [20], which, probably, leads to the fact that the region of the temperature range under investigation lies above the high-temperature boundary of the retrograde solubility region.

4. CONCLUSIONS

The performed investigation of the phase diagram and the structure of the Fe_xTiTe_2 system allows us to conclude that the classical approaches, which take into account only the interaction of atoms with the averaged medium of the solvent, do not explain the observed shape of both the boundary of solubility of iron in Fe_xTiTe_2 and the complex concentration dependences of the lattice parameters. For an adequate description of these dependences, it is necessary to take into account the partial contribution of the electronic subsystem. Using this approach and taking into account the experimental data on the spectrum of electronic states in the Fe_xTiTe_2 system, we can explain (at least qualitatively) the presence of two minima in the concentration dependence of the lattice parameter c, as well as the temperature of the maximum solubility of iron. The general view of the phase diagram of the Fe_xTiTe_2 system corresponds to the general scheme of the phase diagrams accounting for the electronic contribution to the thermodynamic functions of the material [4]. A comparison with the phase diagram of the Fe_xTiSe_2 system makes it possible to elucidate the influence of the elasticity of the host lattice on the position of the solubility boundary of the intercalant: the higher is the elasticity of the lattice, the lower temperature is the part of the generalized phase diagram of the material containing near the Fermi level the bands of localized states with a strong temperature dependence of the band width which corresponds to the experimental phase diagram.

ACKNOWLEDGMENTS

This study was performed using the equipment of the Center for Collective Use "Ural-M" at the Institute of Metallurgy of the Ural Branch of the Russian Academy of Sciences (Yekaterinburg, Russia) and supported by the Presidium of the Ural Branch of the Russian Academy of Sciences (interdisciplinary project no. 12-M-23-2031), the Presidium of the Russian Academy of Sciences (project no. 12-R-2-1051), and the Ministry of Education and Science of the Russian Federation (state contract no. 02.740.11.0821).

REFERENCES

1. K. Yamazaki, K. Shimada, H. Negishi, F. Xu, A. Ino, M. Higashiguchi, H. Namatame, M. Taniguchi, M. Sasaki, S. Titova, A. Titov, and Yu. M. Yarmoshenko, Physica B (Amsterdam) **351**, 262 (2004).
2. X. Y. Cui, H. Negishi, S. G. Titova, K. Shimada, A. Ohnishi, M. Higashiguchi, Y. Miura, S. Hino, A. M. Jahir, A. Titov, H. Bidadi, S. Negishi, H. Namatame, M. Taniguchi, and M. Sasaki, Phys. Rev. B: Condens. Matter **73**, 085111 (2006).
3. A. N. Titov, A. V. Dolgoshein, I. K. Bdikin, and S. G. Titova, Phys. Solid State **42** (9), 1610 (2000).
4. A. N. Titov, E. G. Galieva, and O. V. Antonova, Phys. Solid State **52** (6), 1248 (2010).
5. E. G. Shkvarina, V. A. Tsurin, A. N. Titov, S. G. Titova, and O. M. Fedorova, Phys. Solid State **54** (3), 625 (2012).
6. V. G. Pleshchev, A. N. Titov, S. G. Titova, and A. V. Kuranov, Inorg. Mater. **33** (11), 1128 (1997).
7. H. C. Montgomery, J. Appl. Phys. **42**, 2971 (1971).
8. A. A. Titov, A. I. Merentsov, A. E. Kar'kin, A. N. Titov, and V. V. Fedorenko, Phys. Solid State **51** (2), 230 (2009).
9. A. C. Larson and R. B. Von Dreele, *General Structure Analysis System (GSAS)* (Los Alamos Neutron Science Center (LANSCE), MS-H805, Los Alamos National Laboratory, Los Alamos, New Mexico, 1986), NM 87545.
10. O. Yu. Pankratova, L. I. Grigor'eva, R. A. Zvinchuk, and A. V. Suvorov, Zh. Neorg. Khim. **38**, 410 (1993).
11. A. Titov, S. Titova, M. Neumann, V. Pleschev, Yu. Yarmoshenko, L. Krasavin, A. Dolgoshein, and A. Kuranov, Mol. Cryst. Liq. Cryst. **311**, 161 (1998).
12. T. Hibma, in *Intercalation Chemistry*, Ed. by M. S. Wittingham and A. J. Jacobsen (Academic, London, 1982), pp. 285–313.

13. J. Rouxel and R. Brec, Annu. Rev. Mater. Sci. **16**, 137 (1986).
14. M. V. Yablonskikh, A. S. Shkvarin, Yu. M. Yarmoshenko, N. A. Skorikov, and A. N. Titov, J. Phys.: Condens. Matter **24**, 045504 (2012).
15. N. V. Baranov, V. G. Pleshchev, A. N. Titov, V. I. Maksimov, N. V. Selezneva, and E. M. Sherokalova, Nanotekhnika **15**, 15 (2008).
16. A. N. Titov, Yu. M. Yarmoshenko, M. Neumann, V. G. Pleshchev, and S. G. Titova, Phys. Solid State **46** (9), 1681 (2004).
17. A. N. Titov and A. V. Dolgoshein, Phys. Solid State **42** (3), 434 (2000).
18. D. K. G. de Boer, C. F. van Bruggen, G. W. Bus, R. Coehoorn, C. Haas, G. A. Sawatsky, H. W. Myron, D. Norman, and H. Padmore, Phys. Rev. B: Condens. Matter **29**, 6797 (1984).
19. A. V. Postnikov, M. Neumann, St. Plogmann, Yu. M. Yarmoshenko, A. N. Titov, and A. V. Kuranov, Comput. Mater. Sci. **17**, 450 (2000).
20. S. G. Titova and A. N. Titov, Phys. Solid State **49** (1), 63 (2007).
21. E. G. Galieva, O. V. Antonova, P. E. Panfilov, and A. N. Titov, Phys. Solid State **53** (5), 1047 (2011).
22. A. N. Titov, A. N. Skomorokhov, A. A. Titov, S. G. Titova, and V. A. Semenov, Phys. Solid State **49** (8), 1532 (2007).

Translated by O. Borovik-Romanova